Substantial Crystalline Topology in Amorphous Silicon

J. M. Gibson,[1] M. M. J. Treacy,[2,3,*] T. Sun,[1] and N. J. Zaluzec[4]

[1]*Advanced Photon Source, Argonne National Laboratory, 9700 South Cass Avenue, Argonne Illinois 60439, USA*
[2]*Department of Physics, Arizona State University, Tempe, Arizona 85287, USA*
[3]*Department of Materials, Parks Road, University of Oxford, Oxford, OX1 3PH, United Kingdom*
[4]*Electron Microscopy Center, Materials Science Division, Argonne National Laboratory, 9700 South Cass Avenue, Argonne Illinois 60439, USA*

(Received 20 July 2010; published 17 September 2010)

Using electron correlograph analysis we show that coherent nanodiffraction patterns from sputtered amorphous silicon indicate that there is more local crystallinity in unannealed amorphous silicon than was previously suspected. By comparing with simulations for various models we show that within a typical unannealed amorphous silicon film a substantial volume fraction ($> 50\%$) is topologically crystalline with correlation lengths up to 2 nm. Electron correlograph analysis is a variant of the fluctuation electron microscopy technique and its sensitivity to local crystalline ordering is derived from its sensitivity to four-body correlations.

DOI: 10.1103/PhysRevLett.105.125504 PACS numbers: 61.05.jm, 61.43.Dq

Amorphous silicon is an important electronic material whose properties depend on the topological details of its atomic structure. The presence of crystalline topology at medium-range length scales (≥ 1 nm) has long been debated [1], since conventional diffraction explores only short-range two-body distributions [2,3]. Fluctuation electron microscopy (FEM), which examines the statistics of spatially-resolved coherent diffraction to obtain four-body atomic correlations [4,5], confirms that there is medium-range topological order in amorphous silicon that is not present in a continuous random network (CRN) [6,7]. However, because of difficulties inverting FEM data, there remains an ambiguity about the volume fraction of ordered material [8]. In this Letter we develop a new variant of the FEM technique, electron correlograph analysis, which examines angular autocorrelations of coherent nanodiffraction patterns [9–12], and show that within a typical unannealed amorphous silicon film a substantial volume fraction ($> 50\%$) is topologically crystalline with correlation lengths up to 2 nm.

While topological order can be obvious in a picture of a network, many structural techniques, such as diffraction, that are sensitive only to atomic position correlations and not connectivity, can miss topological order if it is constrained to a medium-range length scale (1–3 nm). It is now well recognized that measurements detecting higher-order atomic positional correlations, such as fluctuation electron microscopy, are much more sensitive to the presence of medium-range topology.

Fluctuation electron microscopy examines the mean and the variance of the scattered intensity from small probed sample volumes as a function of scattering vector $\boldsymbol{k}$ and probe size R. A CRN should give an approximately constant normalized diffraction variance, $V(\boldsymbol{k}, R)$, which is defined as

$$V(\boldsymbol{k}, R) = \frac{\langle I^2(\boldsymbol{r}_p, \boldsymbol{k}, R)\rangle_{r_p}}{\langle I(\boldsymbol{r}_p, \boldsymbol{k}, R)\rangle^2_{r_p}} - 1. \quad (1)$$

$I(\boldsymbol{r}_p, \boldsymbol{k}, R)$ is the diffracted intensity distribution from the sample region centered at $\boldsymbol{r}_p$, and the angular brackets represent averages over the ensemble of probed areas. Experimentally, the probe size (resolution) $R = 1.22/Q$ where Q is the reciprocal diameter of the circular probe-forming aperture, neglecting aberrations. The key to the sensitivity of FEM is that it depends on higher-order, four-body, structural correlation functions. Using high-resolution atomic-scale probes is counterproductive in FEM; the normalized variance is maximized when the probed volume width, R, is comparable to the mean structural correlation length Λ of the sample, $R \approx \Lambda$. The correlation length of the ordering can be estimated by FEM, and is typically 1–2 nm for evaporated amorphous silicon (a-Si) [13]. A series of detailed follow-up studies have revealed the ubiquity of ''paracrystalline'' medium-range order in amorphous tetrahedral semiconductors that have not been annealed [14,15]. Paracrystallites are small regions in the a-Si sample that exhibit a crystalline bonding topology, but are strongly deformed. When the topological correlations are significantly longer than about 3 nm, such samples become polycrystalline, exhibiting long-range order, and conventional diffraction and imaging are again the preferred tools for their study. However, the volume fraction of ordered material is hard to estimate reliably because FEM data is hard to invert, and some have suggested that paracrystallinity, while present, is a minority phase [8,16].

Recently, a related approach to examining higher-order correlations has been reexamined by Wochner *et. al.* [12] The angular cross-correlations in coherent x-ray nanodiffraction patterns from a sub-micron-diameter colloidal glass were studied, and the symmetries of small regions

were identified experimentally. This approach has its origins in the work of Clark, Ackerson and Hurd for lasers [9], and Rodenburg, Cowley, and colleagues for electrons [10,17,18]. We have implemented a variant of this technique using the scanning transmission electron microscope (STEM) approach to FEM (STFEM) by collecting a series of coherent nanodiffraction patterns. We find that there is a statistically meaningful incidence of cubic silicon 111 and 222 Friedel-peak correlations, indicating that there is a substantial volume of topologically crystalline silicon within the sample. (Friedel's Law states that, under weak scattering from a real potential, the diffracted intensity exhibits roto-inversion symmetry. Thus, if a hkl reflection appears, then a $\bar{h}\,\bar{k}\,\bar{l}$ reflection appears also.)

In our experiments, a 20-nm thick freestanding a-Si sample, prepared by sputtering at 200 °C onto amorphous carbon, was examined in a Tecnai F20 ST field emission scanning-transmission electron microscope (TEM-STEM) operating at 200 kV. The sample was argon plasma cleaned to remove the carbon support film before observation. The structure of the a-Si film was not affected by this cleaning. These samples have been studied extensively by FEM before, and are typical of paracrystalline a Si [8]. The instrument was operated in nanodiffraction mode using a range of spatially coherent probe sizes, R, between 0.3–2.3 nm. For each probe size a series of 200 coherent nanodiffraction patterns was obtained at different probe positions on the sample. This is the standard approach for STFEM [19]. Figure 1(a) shows a typical a-Si coherent nanodiffraction pattern obtained for a $R = 2.3$ nm probe. The reciprocal diameter, Q, of the probe-forming aperture is indicated by the white disk in the lower left of the figure.

Correlographs reveal the correlations between bright features (speckle) in individual diffraction patterns, and provide new insight. Correlographs, $G(R, k, \phi)$, from the diffraction patterns of each probed region were obtained by first remapping individual nanodiffraction patterns on a polar grid, with coordinates k (reciprocal lattice vector) and ϕ (azimuthal angle). The normalized autocorrelation function along the azimuthal ϕ axis was calculated for each diffraction pattern

$$G(R, \boldsymbol{r}_p, k, \phi) = \frac{\langle I(R, \boldsymbol{r}_p, k, \phi) I(R, \boldsymbol{r}_p, k, \phi + \Delta)\rangle_\Delta}{\langle\langle I(R, \boldsymbol{r}_p, k, \phi) I(R, \boldsymbol{r}_p, k, \phi + \Delta)\rangle_\Delta\rangle_\phi} - 1. \tag{2}$$

Here, Δ is a dummy variable representing integration over the full 360° azimuthal angle for an angular offset of ϕ. $G(R, \boldsymbol{r}_p, k, \phi)$ is similar to the four-point cross-correlation function introduced by Wochner *et al.* [12] For each probe size R, the spatially averaged correlograph over all probed locations $\boldsymbol{r}$ is computed $\Gamma(R, k, \phi) = \langle G(R, \boldsymbol{r}_p, k, \phi)\rangle_{r_p}$.

The correlograph for the coherent nanodiffraction pattern is shown in Fig. 1(b). The logarithm of the azimuthally-averaged mean diffraction intensity for all 200 patterns is displayed in Fig. 1(c). The associated normalized variance plot [Fig. 1(d)] shows the three pronounced signature peaks for paracrystallinity in a-Si, reproducing previous measurements on these samples [8].

For our sample of a-Si, individual correlographs $G(R, \boldsymbol{r}_p, k, \phi)$ for each probed region centered at $\boldsymbol{r}_p$, display pronounced variation (Fig. 2). Strong bands of contrast occur near the 111, 220, and 222 characteristic

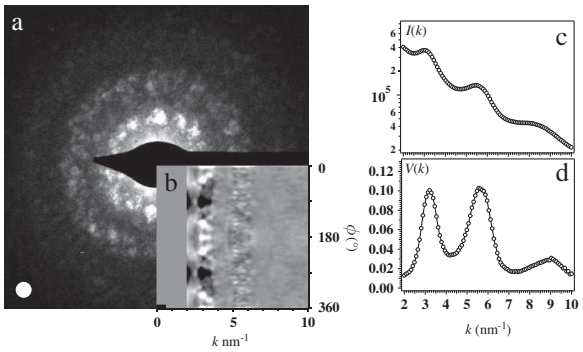

FIG. 1. (a) Typical electron coherent nanodiffraction pattern from the 20-nm thick amorphous silicon film using a probe of nominal resolution 2.3 nm. (b) The associated correlograph. The scattering vector k for both the nanodiffraction pattern and correlograph are aligned on the plot. The vertical axis on the correlograph represents the azimuthal angle ϕ. (c) Logarithm of the azimuthally-averaged mean diffracted intensity versus k for 200 nanodiffraction patterns. (d) Normalized variance plot for this sample, showing the three signature peaks confirming the presence of paracrystallinity.

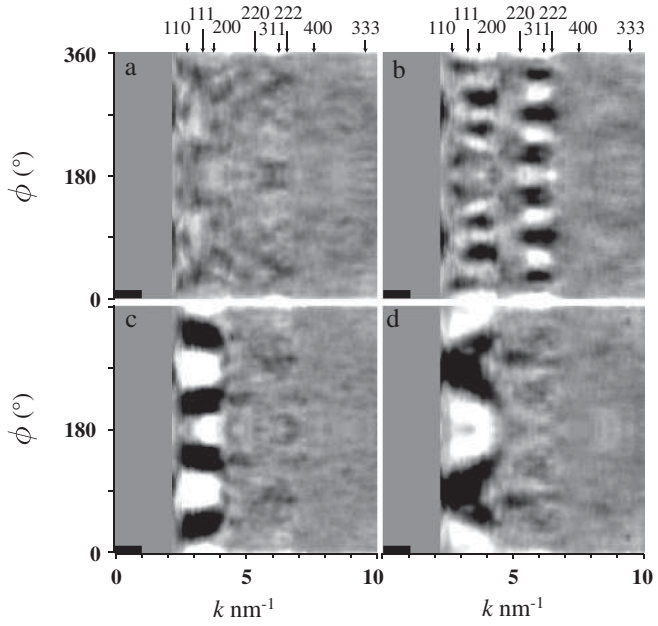

FIG. 2. Typical correlographs taken from four probe positions on the sample for a probe resolution 1.0 nm. Correlographs are highly variable between scanned points and tend to show strong features near scattering vectors corresponding to strong Bragg reflections, hkl, of crystalline cubic silicon. Strong correlations can also occur near forbidden reflections such as 110 and 200. The uniform grey band on the left is from the beam stop. The semiangle subtended by the illumination disk along the k axis is indicated by the black bar.

cubic silicon reflections—evidence of pervasive crystalline topology. No two regions show identical patterns. However, when we average over 200 patterns, the resulting mean correlographs $\Gamma(R, k, \phi)$ are reproducible for a given sample (Fig. 3), and inform us about the average correlations. For high-resolution probes, $R < 0.5$ nm [Fig. 3(a)], we observe essentially no strong correlations. As the probe size approaches $R \sim 1$ nm [Fig. 3(b)] a Friedel peak at $\bar{1}\,\bar{1}\,\bar{1}$ appears at $\phi = 180°$ for k-vectors close to the cubic Si 111 band. In addition, there is evidence of weak $1\bar{1}0$ and 020 at $\pm 90°$ to the nominally-forbidden 110 and 200 reflections. As the probe size becomes larger [Figs. 3(c) and 3(d)], the Friedel $\bar{1}\,\bar{1}\,\bar{1}$ peak gets stronger and a $\bar{2}\,\bar{2}\,\bar{2}$ Friedel peak appears at the 222 band as an arc, and the forbidden reflections fade. A weak $\bar{3}\,\bar{1}\,\bar{1}$ correlation appears, but no strong Friedel $\bar{2}\,\bar{2}\,0$ correlation appears at the 220 band. These details are consistent with the presence of twinning on the 111 planes, introducing a hexagonal topology, which attenuates some of the 220 reflections and allows intensity at the 110 and 200 positions. The arc shape at higher k has been explained by Rodenburg [20] in terms of the Ewald sphere intercepting higher-order Laue zone reflections of the diffraction disk, which are generated by ordered regions in the sample. In random samples (such as a CRN), Friedel's law does not often apply to bright diffraction spots because the Ewald sphere curvature is high compared with the inverse of the specimen thickness. However, compact ordered regions are sufficiently extended in reciprocal space that Friedel's law most often applies to their diffracted beams.

To understand these results, a simple model of paracrystalline silicon was made by first filling space with random points and then constructing the Voronoi tessellation. The spread of Voronoi volumes follows a gamma distribution. For a given mean volume, each randomly selected Voronoi region was filled with either a randomly oriented cubic silicon structure, or a randomly picked fragment from a large CRN structure [21]. No attempt was made to relax grain boundaries [22], but no atom distance closer than 0.2 nm was allowed. The model density agreed well with that for amorphous silicon. A 40×40 array of kinematical diffraction patterns from models of various thicknesses, mean grain sizes and probe sizes were computed as a function of the percentage crystalline fill-factor. The mean intensity $\langle I(\boldsymbol{r}_p, \boldsymbol{k}, R)\rangle_{r_p}$, normalized variance $V(\boldsymbol{k}, R)$, and mean correlograph $\Gamma(R, k, \phi)$ were computed. Results show that a CRN model can not explain the experimental correlographs. Computations for 1.2-nm mean-diameter grains, 20-nm thickness, and probe size $R = 1.0$ nm, are presented in Fig. 4. For this model, the best overall visual fit to the experimental data, occurs for high crystalline fill factors $\geq 65\%$ [Fig. 4(c)]. This value depends on the model parameters, but it is clear our a-Si material is substantially crystalline at the 1–2 nm length scale.

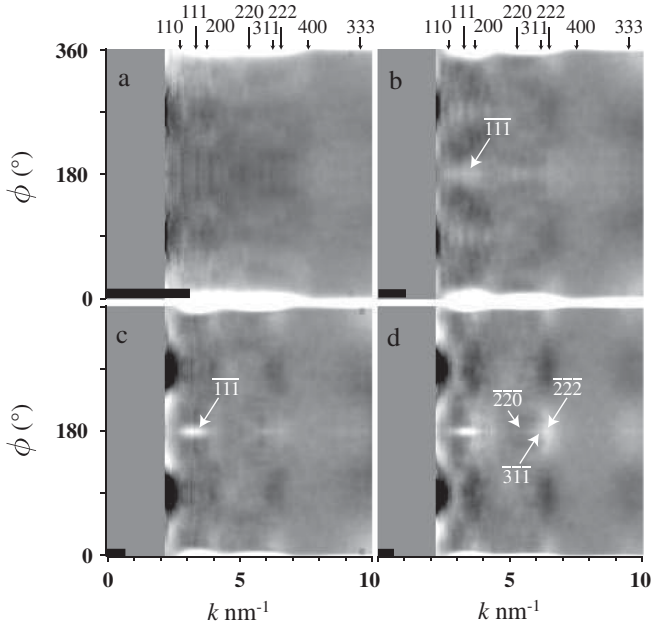

FIG. 3. Mean correlographs, averaged over 200 probed positions for four different probe resolutions, R. (a) $R = 0.3$ nm. (b) $R = 1.0$ nm. (c) $R = 1.5$ nm. (d) $R = 2.3$ nm. The high-resolution correlograph, (a), shows little correlation. The lower-resolution correlographs (b),(c), and (d) show strong 180° Friedel correlations between the 111 and $\bar{1}\,\bar{1}\,\bar{1}$ peaks, and the 222 and $\bar{2}\,\bar{2}\,\bar{2}$ Friedel peaks. The semiangle subtended by the illumination disk is indicated by the black bar.

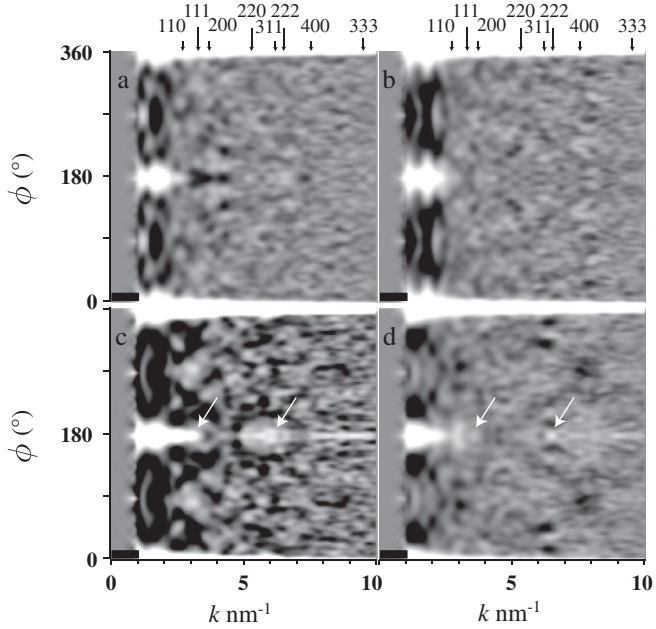

FIG. 4. Simulated mean correlographs for a model amorphous system with randomly-oriented unstrained cubic crystalline grains of mean diameter 1.2 nm, arranged in a thin film made from a CRN of thickness 20 nm. (a) 0% crystalline, 100% CRN. (b) 35% crystalline grains, 65% CRN. (c) 65% crystalline grains, 35% CRN. (d) 100% crystalline grains, 0% CRN. The higher crystallinity models, $\geq 65\%$, reproduce the $\bar{1}\,\bar{1}\,\bar{1}$ and $\bar{2}\,\bar{2}\,\bar{2}$ Friedel peaks in the data best (indicated).

For thin samples, <10 nm, simulations exhibit strong Friedel correlations, including $\bar{2}\,\bar{2}\,0$ and $\bar{4}00$ correlation peaks that do not occur strongly in our *a*-Si data. These are suppressed when strain and twinning is added to our model. Thicker models also suppress these, as seen in Fig. 4 for 20 nm thickness. In each case, the $\bar{1}\,\bar{1}\,\bar{1}$ and $\bar{2}\,\bar{2}\,\bar{2}$ Friedel correlations persist.

The presence of Friedel correlations provides an important clue. Friedel's law breaks down for thicker crystallites, and when the scattered wave front is randomized by thick disordered samples where the weak phase object approximation is not valid [20]. Their persistence in the mean correlographs indicates that there is nonrandom, correlated, scattering in the *a*-Si sample—the fingerprint of medium-range order. Individual simulated correlographs exhibit fascinating structure, with bright and dark bands crossing the correlograph at various angles. Wochner *et al.* observed fivefold and tenfold symmetries in their colloidal glass [12]. No such fivefold and tenfold symmetry was observed in our silicon data.

Individual correlographs confirm that there is significant crystalline topology in every probed region. The $\bar{1}\,\bar{1}\,\bar{1}$ and $\bar{2}\,\bar{2}\,\bar{2}$ reflections likely persist because they are common to both the cubic and hexagonal topologies. Analysis shows that at least 65% of our sample can be modeled as undisturbed, 1-nm diameter, cubic Si grains.

Three key aspects of FEM are preserved in the diffraction correlograph approach. First, there is control of the probe size *R* to ensure adequate sampling of the correlated material. This was one reason why the earlier electron diffraction experiments missed correlations in amorphous Si [10]. Second, it is a statistical approach rather than an attempt to identify individual, and probably unrepeatable, features. Third, there is access to information about four-body correlations since both methods examine intensity-intensity correlations. Information about higher-order correlations will be found in the correlograph variance.

As we have learned from FEM studies, four-body measures of diffraction data are hard to invert to obtain models. Generally, models are guessed and simulations are made, which rely heavily on good guesses. Monte Carlo-type methods are showing much promise for data inversion [23,24], with both diffraction and variance data constraining the structural relaxation. Correlographs depend sensitively on the model details, and would provide valuable additional constraints to such methods.

Electron correlograph analysis offers a complementary approach to FEM for exploring medium-range order, when performed in a STEM. Variable resolution FEM provides the length scale of paracrystalline ordering [13]. Now electron correlograph analysis provides a way to quantify the extent of that paracrystallinity. In this study, correlograph modelling confirms that there is substantial crystalline topology in the *a*-Si sample studied here, over 65%, and that as-deposited *a*-Si is not well represented by a random network. This has significant implications for our understanding of structure and properties in amorphous semiconductors and related materials.

M. M. J. T is grateful for support from the Leverhulme Trust. We acknowledge support from the Advanced Photon Source, and the Electron Microscopy Center, at Argonne National Laboratory, U. S. Department of Energy, Contract No. DE-AC02-06CH11357. We thank J. R. Abelson and B. S. Lee of the University of Illinois, Urbana-Champaign, for providing the samples.

*treacy@asu.edu

[1] J. S. Lannin, Phys. Today **42**, No. 6, 115 (1989).
[2] J. Fortner and J. S. Lannin, Phys. Rev. B **39**, 5527 (1989).
[3] D. J. H. Cockayne, Annu. Rev. Mater. Res. **37**, 159 (2007).
[4] M. M. J. Treacy and J. M. Gibson, Acta Crystallogr. Sect. A **52**, 212 (1996).
[5] M. M. J. Treacy, J. M. Gibson, L. Fan, D. J. Paterson, and I. McNulty, Rep. Prog. Phys. **68**, 2899 (2005).
[6] J. M. Gibson and M. M. J. Treacy, Phys. Rev. Lett. **78**, 1074 (1997).
[7] J. M. Gibson and M. M. J. Treacy, J. Non-Cryst. Solids **231**, 99 (1998).
[8] S. N. Bogle, P. M. Voyles, S. V. Khare, and J. R. Abelson, J. Phys. Condens. Matter **19**, 455204 (2007).
[9] N. A. Clark, B. J. Ackerson, and A. J. Hurd, Phys. Rev. Lett. **50**, 1459 (1983).
[10] A. Howie, C. A. McGill, and J. M. Rodenburg, J. Phys. (Paris) **46**, C9-59 (1985).
[11] G. Y. Fan and J. M. Cowley, Ultramicroscopy **17**, 345 (1985).
[12] P. Wochner, C. Gutt, T. Autenrieth, T. Demmer, V. Bugaev, A. D. Ortiz, A. Duri, F. Zontone, G. Gruebel, and H. Dosch, Proc. Natl. Acad. Sci. U.S.A. **106**, 11 511 (2009).
[13] J. M. Gibson, M. M. J. Treacy, and P. M. Voyles, Ultramicroscopy **83**, 169 (2000).
[14] J. M. Gibson, J.-Y. Cheng, P. M. Voyles, M. M. J. Treacy, and D. C. Jacobson, in *Microstructural Processes in Irradiated Materials*, edited by S. J. Zinkle, G. Lucas, and R. Ewing (Materials Research Society, Pittsburgh, PA, 1999), Vol. 540, p. 27.
[15] J. E. Gerbi, P. M. Voyles, M. M. J. Treacy, J. M. Gibson, and J. R. Abelson, Appl. Phys. Lett. **82**, 3665 (2003).
[16] A. F. I. Morral and P. R. I. Cabarrocas, Thin Solid Films **383**, 161 (2001).
[17] J. M. Rodenburg, J. Phys. (Paris) **46**, C9-63 (1985).
[18] J. M. Rodenburg and I. A. Rauf, Inst. Phys. Conf. Ser. No. **98**, 119 (1990).
[19] P. M. Voyles and D. A. Muller, Ultramicroscopy **93**, 147 (2002).
[20] J. M. Rodenburg, Ultramicroscopy **25**, 329 (1988).
[21] G. T. Barkema and N. Mousseau, Phys. Rev. B **62**, 4985 (2000).
[22] S. M. Nakhmanson, P. M. Voyles, N. Mousseau, G. T. Barkema, and D. A. Drabold, Phys. Rev. B **63**, 235207 (2001).
[23] P. Biswas, D. N. Tafen, and D. A. Drabold, Phys. Rev. B **71**, 054204 (2005).
[24] J. Hwang, A. M. Clausen, H. Cao, and P. M. Voyles, J. Mater. Res. **24**, 3121 (2009).